

Received September 9, 2020, accepted September 17, 2020, date of publication September 21, 2020, date of current version October 5, 2020.

Digital Object Identifier 10.1109/ACCESS.2020.3025575

Anti-Disturbance Direct Yaw Moment Control of a Four-Wheeled Autonomous Mobile Robot

LIQUAN JIANG¹, SHUTING WANG¹, YUANLONG XIE¹, (Member, IEEE), JIE MENG¹, SHIQI ZHENG^{1,2,3}, XIAOLONG ZHANG¹, (Student Member, IEEE), AND HAO WU¹

¹School of Mechanical Science and Engineering, Huazhong University of Science and Technology, Wuhan 430074, China

²School of Automation, China University of Geosciences, Wuhan 430074, China

³Hubei Key Laboratory of Advanced Control and Intelligent Automation for Complex Systems, Wuhan 430074, China

Corresponding author: Yuanlong Xie (yuanlongxie@hust.edu.cn)

This work was supported in part by the National Key Research and Development Project under Grant SQ2020YFB170258, in part by the China Postdoctoral Science Foundation under Grant 2019M650179, in part by the Hubei Technical Innovation Project under Grant 2018AAA027, in part by the Guangdong Major Science and Technology Project under Grant 2019B090919003, in part by the Launch Fund of Huazhong University of Science and Technology (02), and in part by the National Natural Science Foundation of China under Grant 61703376 and Grant 51675197.

ABSTRACT Profiting from its remarkable maneuverability and efficiency, the four-wheeled autonomous mobile robot (FAMR) is appealing for intelligent manufacturing and automation applications. However, the suppression of unknown disturbances and system uncertainties remains a challenge for formulating a precise trajectory-tracking control scheme. This paper achieves the anti-disturbance direct yaw moment control of a developed FAMR by proposing a robust super-twisting sliding mode controller (RSSMC) to enhance the dynamic tracking and disturbance rejection property simultaneously. One of the major contributions is that the presented RSSMC method is constructed with a novel reaching law to eliminate the matched perturbations and time-varying lumped disturbances. As another distinguishing feature, this method is capable of driving the resultant FAMR trajectory into a bounded switching region and maintaining it therein for subsequent periods in finite time. To guarantee the closed-loop stability and finite-time convergence, new sufficient conditions for specifying the variable gains are determined utilizing Lyapunov functions. Finally, under the direct yaw moment control framework, simulation experiments of a developed FAMR system are offered to verify the practicability of the RSSMC scheme.


INDEX TERMS Direct yaw moment control, four-wheeled autonomous mobile robot, super-twisting sliding mode controller, anti-disturbance.

I. INTRODUCTION

Compared to other automation technologies, which require more time and effort to retrofitting and renovating, mobile robots can be flexibly switched to perform new tasks with relative ease [1]–[3]. With all-wheel independently steering and actuating features, the four-wheeled autonomous mobile robot (FAMR) is able to dynamically optimize its efficient pathways to achieve flexible and agile automation [4], [5]. As shown in Figure 1, a practical FAMR is potential for transferring the workpieces between different machining units in manufacturing factories or mobile processing of large complex parts [6], [7]. Equipped with mecanum or omni wheels, the traditional FAMR ensures the wheels and

rollers an active rotation to enable superb moving capability in arbitrary directions [8]. However, mecanum wheels have rigid requirements for the ground flatness, which is not applicable to rough terrains or greasy surfaces. However, this normally occurs in typical manufacturing scenarios [9], [10]. To address these limitations, a FAMR with a car-wheeled structure can be independently actuated by in-wheel-driven motors, thus maintaining its free orientation regulation of the four-wheeled actuation system while offering better tolerance to surface irregularity and higher durability of tires [11]–[13]. In this regard, it achieves higher maneuverability and adaptability when applying to uneven or confined operating environments.

To enhance the existing industrial solutions of FAMR, some prior researches have been developed to stabilize the FAMR systems via advanced control strategies [14], [15].

The associate editor coordinating the review of this manuscript and approving it for publication was Pedro Neto .

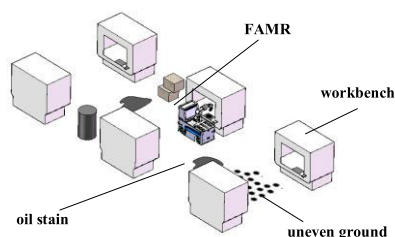


FIGURE 1. The typical the manufacturing scenario.

As a primary step, a kinematic model or dynamic model is needed to be identified for formulating a kinematic or dynamic control scheme, respectively [16]–[18]. It is well known that a kinematic design retains the control simplicity and accuracy concurrently [19]. However, the achieved performance may be mitigated since the dynamics and actuation forces are not considered when deriving a control law for complex operating environments (e.g., non-idealized ground/wheel interactions). In comparison, the chassis dynamic control of the FAMR can reach a precise direct yaw moment regulation, leading to improved tracking features concerning asymptotical convergence and stability [20], [21]. Up to now, various studies have been presented, focusing on the direct yaw moment control of mobile robots. For optimizing the desired yaw moment and active steering angle, a multi-objective model predictive controller is designed to allocate the four-wheel torques with guaranteed closed-loop stability [22]. By utilizing a robust control framework, Hu *et al.* address the motion stabilization issue of four-wheel electric vehicles subject to model uncertainties, external disturbances, and parameter variations [23]. To optimize the yaw moment distribution, a hierarchical strategy is proposed by integrating an overlook controller and a servo-loop controller to resolve the yaw moment and torque distribution, separately [24].

It is noted that sliding mode control (SMC) can achieve superior advantages of insensitivity to system uncertainties, quick tracking response and easy to implement [25]–[29]. There have been some interesting SMC solutions for the existing control issues, such as the systems subject to randomly occurring mixed time-delays under uncertain occurrence probabilities [26], [29]. Till now, SMC has been incorporated into direct yaw moment control systems over recent years. For instance, Ding *et al.* optimize the yaw moment adaption law by combining the sliding mode mechanism and disturbance observer technology [30]; An integral SMC solution is proposed to achieve a torque-vectoring regulation scheme for electric vehicles with practical demonstrations [31]. Indeed, the promising SMC solutions can enhance the control capabilities from both uncertain and time-varying disturbance alleviation and asymptotical stability. However, there exist some synthesis problems remain to be resolved for direct yaw moment control of an in-wheel-driven FAMR:

- 1) *Multiple allocations of four-wheeled configuration.* It should be mentioned that the concerned FAMR system

with the four independently in-wheel-driven ability can be operated in various single-track dynamic modes. The typical modes include Ackerman mode (the traditional car-like mode), double-Ackerman mode, diagonal-move mode and zero-radius steer mode, etc [32]–[34]. Given this context, the alternative FAMR can be further employed for various applications due to the enhanced practicability in clustered spaces and confined scenes [19]. However, most of the existing direct yaw moment control schemes are only applicable to car-like electric vehicles [14], [35]–[37], implying that only the traditional Ackerman mode is applicable for real-world implementations. Naturally, a question is raised here: How can we derive a more universal lateral motion control framework for the FAMR with variable configurable modes?

- 2) *Chattering-free disturbances suppression issue.* Non-ignorable high chattering activities will be resulted from the discontinuous control mechanism of traditional sliding mode mechanism. A possible way to mitigate the undesirable chattering is to revise the enforcement law through designing a specialized function related to the desired sliding surfaces, such as the boundary layer or some smoother terms [12]. However, a trade-off between enhancing the tracking performance and strengthening the system robustness is imposed on optimizing a practical smooth reaching law [10], [38], [39]. Although the traditional constant proportional rate law can obtain a fast response, its limited stability implies that it is not suitable for a disturbed system [40]; the power rate reaching law is able to improve the resultant robustness because of the natural lessening property of its employed exponential term [41]. For a practical SMC design, the disturbance rejection capacity should be considered during the derivation of enforcement laws to enhance the dynamic control precision. To this end, the related control parameters may be overestimated to handle the unknown disturbances and uncertainties, leading to anabatic chattering phenomena. Up to now, exploring an optimal solution with chattering-free dynamic tracking and disturbance rejection abilities is of great significance to achieve well-pleasing control effects for the potential industrial applications of the FAMR.

Based on the previous discussions, this paper presents a robust super-twisting sliding-mode controller (RSSMC) to derive the direct yaw moment control framework of the considered FAMR, realizing simultaneous dynamic tracking and disturbance rejection. Compared to the existing studies, major contributions can be reflected in:

- 1) In contrast to traditional control designs of FAMR, the presented method is more universal in two aspects:
 - a.* The optional multi-mode of the chassis motion can be configured to achieve flexible torque distribution, gaining more adaptivity in a complex environment;
 - b.*

the unknown disturbances and uncertainties are considered simultaneously, including the unmodelled dynamics and time-varying parametric vibrations.

- 2) A novel anti-disturbance mechanism is proposed, which is capable of handling the time-varying perturbations and the discontinuity chattering. Given this context, the chattering phenomenon in traditional solutions can be effectively handled with the derived reaching law, and sufficient conditions for the multivariable gains are formulated to ensure the lateral motion control stability and finite-time convergence.
- 3) The presented RSSMC method is easy for practical implementation. Comparison simulation experiments are carried out in real-world scenarios, validating the benefits and superior abilities of the proposed method.

The rest is constructed as follows. The system modelling and problem statement are clarified in Section 2. Section 3 gives the proposed RSSMC framework with guaranteed stability and finite-time convergence. Section 4 provides the validation results and analysis while Section 5 offers the research conclusions and future working directions.

II. PROBLEM STATEMENT

A. SYSTEM MODELLING

With interconnected variables, the dynamic states of the developed FAMR can be formulated as a nonlinear multiple-input multiple-output system. Figure 2 shows the two-degree-of-freedom planar model of the considered FAMR system. Specially, for the yaw plane representation, the nonlinear four-wheel formulations of the concerned FAMR can be expressed by

$$m v_x (\dot{\beta} + \gamma) = \sum_{i=1}^2 (F_i^x \sin \delta_f + F_i^y \cos \delta_f) + \sum_{i=3}^4 (F_i^y \cos \delta_r - F_i^x \sin \delta_r) \quad (1)$$

$$I_z \dot{\gamma} = \sum_{i=1}^2 l_f (F_i^x \sin \delta_f + F_i^y \cos \delta_f) - \sum_{i=3}^4 l_r (F_i^y \cos \delta_r - F_i^x \sin \delta_r) + M_\omega \quad (2)$$

where m denotes the total mass of the FAMR, v_x denotes the longitudinal speed at the centre of gravity (CG), F_i^x and F_i^y are the longitudinal and lateral tire forces at i th tire, respectively, β and γ denote the sideslip angle and yaw rate, separately, I_z is the inertia moment, l_f and l_r denote the distances from the front and rear axles, respectively, δ_f and δ_r are the virtual front wheel and rear wheel angles, respectively, M_ω denotes the yaw moment generated by the traction moment of four wheels, i.e.,

$$M_\omega = 0.5d(F_{rr}^x - F_{rl}^x) \cos \delta_r + 0.5d(F_{fr}^x - F_{fl}^x) \cos \delta_f \quad (3)$$

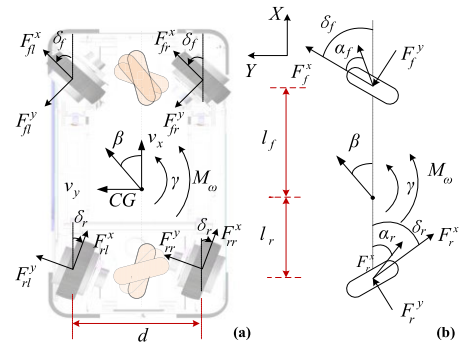


FIGURE 2. The two-degree-of-freedom planar model of the considered FAMR system. (a) Four-wheel presentation; (b) Single-track presentation.

where d denotes the track width, F_{rr}^x , F_{rl}^x , F_{fr}^x and F_{fl}^x denote the longitudinal tire forces acting on the rear-left tire, rear-left tire, front-right tire, and front-left tire, respectively.

In practice, we can directly measure or estimate F_{rr}^x , F_{rl}^x , F_{fr}^x and F_{fl}^x using observer techniques [35]. Note that for a general system, we can describe the δ_r use $\delta_r = k \delta_f$, where k is a user-defined coefficient that can be used for operating model configuration. For example, by specifying $k = 1$, the turning radius under double-Ackerman mode can be decreased by 35%, enhancing the practicability and superiority for desired profiles with distinct curvature vibrations [36]. Without loss of generality, we define

$$k = \begin{cases} 0 & \text{Ackerman mode} \\ 1 & \text{Double-Ackerman mode} \\ -1 & \text{Diagonal-move steer mode} \\ (0, 1) & \text{Variable Ackerman mode} \end{cases} \quad (4)$$

As shown in Figure 2(b), for the dynamic RSSMC controller design, one can simplify the four-wheel model as a single-track mode. As demonstrated in (4), unlike the traditional yaw moment vehicle model, we introduce the user-defined coefficient k into the construction of a single-track model to achieve a uniform yaw moment control model. With the virtual front and rear wheels, we rewrite the lateral and yaw dynamics as

$$m v_x (\dot{\beta} + \gamma) = F_f^y \cos \delta_f + F_r^y \cos \delta_r \quad (5)$$

$$I_z \dot{\gamma} = l_f F_f^y \cos \delta_f - l_r F_r^y \cos \delta_r + M_\omega \quad (6)$$

where the lateral tire forces F_f^y and F_r^y can be linearly calculated as follows

$$F_f^y = -C_f \left(\beta + \frac{l_f \gamma}{v_x} - \delta_f \right) \quad (7)$$

$$F_r^y = -C_r \left(\beta - \frac{l_r \gamma}{v_x} + \delta_r \right) \quad (8)$$

where C_f and C_r denote the cornering stiffnesses of the front and rear tires, separately.

In general, the tire concerning stiffness is affected by weight transfer. By applying small-angle approximation (e.g., $\cos \delta_f \approx 1$, $\cos \delta_r \approx 1$), we reconstruct the nonlinear

dynamic model derived by (5)-(8) in a general form

$$\dot{x}(t) = Ax(t) + Bu(t) + f(x, t) \quad (9)$$

where $x(t) = [\beta, \gamma]^T$ and $u(t) = [\delta_f, M_\omega]^T$ denote the vectors of system state and control input, respectively, $f(x, t)$ denotes the external disturbance, and the corresponding parametric vectors A and B are obtained as

$$A = \begin{bmatrix} \frac{-(C_f + C_r)}{mv_x} & \frac{(l_r C_r - l_f C_f)}{mv_x^2} - 1 \\ \frac{-(l_f C_f - l_r C_r)}{I_z} & \frac{-(l_f^2 C_f + l_r^2 C_r)}{I_z v_x} \end{bmatrix}$$

$$B = \begin{bmatrix} \frac{C_f - C_r k}{mv_x} & 0 \\ \frac{l_f C_f + l_r C_r k}{I_z} & \frac{1}{I_z} \end{bmatrix}$$

Then, considering the parametric perturbation, one can further construct the FAMR system (9) as

$$\dot{x}(t) = (\hat{A} + \Delta A)x(t) + (\hat{B} + \Delta B)u(t) + f(x, t) \quad (10)$$

where \hat{A} and \hat{B} stand for the nominal matrix derived from using $C_f = \hat{C}_f$ and $C_r = \hat{C}_r$, \hat{C}_f and \hat{C}_r are the related nominal parameters, ΔA and ΔB are the uncertainties caused by the vibrations of the tire concerning stiffness.

By using the parametric perturbation $d(x, t)$ as

$$d(x, t) = \Delta Ax(t) + \Delta Bu(t) \quad (11)$$

we can define a lumped disturbance as

$$D(x, t) = d(x, t) + f(x, t) \quad (12)$$

For a practical, one can further assume that $D(x, t)$ and the related derivative $\dot{D}(x, t)$ are bounded by respective known positive constants D_m and \dot{D}_m , which implies that

$$\|D(x, t)\| < D_m \quad (13)$$

$$\|\dot{D}(x, t)\| < \dot{D}_m \quad (14)$$

Hence, the considered system can be finally expressed by

$$\dot{x}(t) = \hat{A}x(t) + \hat{B}u(t) + D(x, t) \quad (15)$$

B. PROBLEM STATEMENT

In practice, the yaw rate and sideslip angle have been regarded as the universally applied indicators of lateral stability and dynamic performance. Note that it can be achieved by independent in wheel-motor control of the FAMR. Given this context, the trajectory-tracking problem considered in this work is translated into the direct yaw moment control issue of the FAMR to stabilize the lateral motion activities. To this end, this paper aims at designing an RSSMC control scheme for the disturbed FAMR system, realizing the lateral stability control when following the desired profiles. In this paper, the required yaw rate γ_d is attained on the basis of the desired trajectories (thus γ_d is time-varying) assuming the controlled system is with widely-employed Ackerman mode. Specifically, we will use a convenient reference model for

the considered FAMR based on the known information, such as the steering angle and longitudinal velocity. To be more specific, the concerning γ_d of the vehicle can be determined by

$$\gamma_d = \min\{|\gamma_1|, |\gamma_{\max}|\} \cdot \text{sign}(\delta_f) \quad (16)$$

where $|\gamma_{\max}| = \mu g/v_x$ with μ being the road adhesion coefficient, and γ_1 is determined by

$$\gamma_1 = \frac{v_x/d}{1 + K v_x^2} \delta_f, \quad K = \frac{m}{2d^2} \left(\frac{L_f}{C_r} - \frac{L_r}{C_f} \right) \quad (17)$$

Generally speaking, the yaw rate can be affected more easily by the control decisions and actuation system of the FAMR. This implies that it is more sensitive to the stability of lateral motion control. In comparison, as the embodiment of the tire slip angles on the robotic main body, the reference sideslip angle is normally assumed to be around its minimum, which is determined by zero in this paper to enhance the lateral motion control stability [42]. On the other hand, different from the traditional method, which assumes the ideal system modelling and identifications, the parametric perturbation and unknown disturbances are considered in the FAMR dynamic responses here. To this end, we will formulate a robust controller to make the yaw rate and sideslip angle approach their respective desired values, which can enhance the dynamic tracking and disturbance rejection property simultaneously.

III. THE PROPOSED RSSMC METHOD

To begin with, suppose that (A, B) is controllable and the matrix B has full column rank. Specially, we use n and m to denote the general dimensional of the input vector and output vector, respectively. Then, we define

$$z = [z_1(t) \quad z_2(t)]^T = \mathcal{F}x \quad (18)$$

where $z_1(t) \in R^{n-m}$, $z_2(t) \in R^m$, $\mathcal{F} = [B_1 \quad B_2]^T$, $B_1 B = 0$, $B_2 = (B^T B)^{-1} B^T$.

Then, the system described by (10) can be transformed into

$$\dot{z} = \tilde{A}z + [0 \quad u(t) + \tilde{f}(x, t)]^T \quad (19)$$

where $\tilde{f}(x, t)$ denotes the continuous uncertainties/ disturbances and $\tilde{A} = \mathcal{F}A\mathcal{F}^{-1}$ can be expressed by

$$\tilde{A} = \begin{bmatrix} \tilde{A}_{11} & \tilde{A}_{12} \\ \tilde{A}_{21} & \tilde{A}_{22} \end{bmatrix} \quad (20)$$

with elements

$$\tilde{A}_{11} \in R^{(n-m) \times (n-m)}, \quad \tilde{A}_{12} \in R^{(n-m) \times m},$$

$$\tilde{A}_{21} \in R^{m \times (n-m)}, \quad \tilde{A}_{22} \in R^{m \times m}$$

Therefore, one can re-present the corresponding hybrid system (19) using

$$\begin{bmatrix} \dot{z}_1(t) \\ \dot{z}_2(t) \end{bmatrix} = \begin{bmatrix} \tilde{A}_{11} & \tilde{A}_{12} \\ \tilde{A}_{21} & \tilde{A}_{22} \end{bmatrix} \begin{bmatrix} z_1(t) \\ z_2(t) \end{bmatrix} + \begin{bmatrix} 0 \\ u(t) + \tilde{f}(x, t) \end{bmatrix} \quad (21)$$

The desired sliding mode surface of this paper is constructed as

$$s = z_2 - Gz_1 \tag{22}$$

where $G \in R^{m \times (n-m)}$ is a matrix to be designed later.

Together with the equivalent law u_{eq} , the control input takes the form of

$$u = u_{eq} + \varpi(s) + v \tag{23}$$

$$\varpi(s) = -(\tilde{A}_{22} - G\tilde{A}_{12})s \tag{24}$$

where v denotes the enforcement control law.

To obtain the equivalent law u_{eq} , the integration of $s = 0$ and (22) leads to a reduced model

$$\begin{cases} \dot{z}_1(t) = \tilde{A}_{11}z_1(t) + \tilde{A}_{12}Gz_1(t) \\ \dot{z}_2(t) = \tilde{A}_{21}z_1(t) + \tilde{A}_{22}Gz_1(t) + \tilde{f}(x, t) + u(t) \end{cases} \tag{25}$$

Thus, one can determine u_{eq} using

$$u_{eq} = -(\tilde{A}_{21} + \tilde{A}_{22}G - G(\tilde{A}_{11} + \tilde{A}_{12}G))z_1(t) \tag{26}$$

On the other hand, with

$$\phi_1(s) = \mu_1|s|^{1/2}sign(s) + \mu_2s \tag{27}$$

where $\mu_{i=1,2} > 0$ denote pre-defined coefficient, the sliding mode reaching conditions can be satisfied by applying the enforcement law as below

$$v = -\sigma_1\phi_1(s) - \sigma_2\phi_2(s) \tag{28}$$

$$\begin{aligned} \dot{\phi}_2(s) &= \dot{\phi}_1(s)\phi_1(s) \\ &= \frac{d}{dt}(\mu_1|s|^{0.5}sign(s) + \mu_2s) \\ &\quad \cdot (\mu_1|s|^{0.5}sign(s) + \mu_2s) \\ &= 0.5\mu_1^2sign(s) + 1.5\mu_1\mu_2|s|^{0.5}sign(s) + \mu_2^2s \end{aligned} \tag{29}$$

where σ_1 and σ_2 are the related control gains.

It is mentioned that if $\mu_1 = 1, \mu_2 = 0$, we may consider (28) and (29) as the normal form of the traditional super-twisting algorithm [43], [44], which can achieve a continuous control scheme. However, it cannot cope with the undesired perturbations. In another case, by setting $\mu_1 = 0, \mu_2 = 1$, one can realize a linear implementation of SMC solution with the help of symbolic function. In this paper, by employing $\mu_{i=1,2} > 0$, we can handle the perturbations growing linearly in s . The potential control gains (i.e., σ_1 and σ_2) provide an opportunity to improve the insensitivity of the sliding surface to perturbations and disturbances increasing. This implies that the control variable derived in this paper is absolutely continuous as compared with the discontinuous characteristics of conventional SMC solutions.

Remark 1: In practice, the corresponding matrix G can be determined by utilizing linear control methods, e.g., eigenvalue assignment (adopted here) and optimal control approaches. It is pointed out that the selection of G may affect the approaching rate of the desired sliding manifold ($s = 0$). However, the closed-loop stability of the resultant system

will not be influenced. Generally, the elements of matrix G can help the FAMR system to satisfy the requirements of dynamic trajectory tracking. For example, by using the eigenvalue assignment method to obtain G , one can pre-specify the system eigenvalues to obtain the required dynamic response. Further, with the linear quadratic regulator method, it is possible to achieve an optimal sliding manifold by constructing and optimizing a cost function related to the system state variables [45].

Theorem 1: Supposing the FAMR system is under the control of the proposed RSSMC law determined by (23), (24), (26) and (28), there exists a range of values $\sigma_{i=1,2}$ such that both the designed sliding surface s and its derivative \dot{s} are converged to the origin in finite time and maintain on it during the succedent periods. That is to say, under the proposed method, the closed-loop stability of the resultant FAMR system can be guaranteed.

Proof: The proof is split into the following two steps.

In the first step, we will present the sliding mode surface in a form that is convenient for Lyapunov analysis.

According to (21) and (22), one can reformulate the transformed lumped disturbance $\tilde{f}(x, t)$ as follows

$$\begin{cases} \tilde{f}(z_1, z_2 + Gz_1, t) = g_1(z_1, s, t) + g_2(z_1, t) \\ g_1(z_1, s, t) = \tilde{f}(z_1, z_2 + Gz_1, t) - \tilde{f}(z_1, Gz_2, t) \\ g_2(z_1, t) = \tilde{f}(z_1, Gz_2, t) \end{cases} \tag{30}$$

Since the lumped disturbance, together with its derivative, are assumed to be bounded in this paper, one can obtain the following inequalities

$$\begin{aligned} |g_1(z_1, s, t)| &\leq \mathcal{B}_1(t, x)|\phi_1(s)| \\ &= \mathcal{B}_1(t, x)|\mu_1|s|^{1/2}sign(s) + \mu_2s| \\ &= \mathcal{B}_1(t, x)[\mu_1 + \mu_2|s|^2]|s|^{1/2} \end{aligned} \tag{31}$$

$$\begin{aligned} \left| \frac{d}{dt}g_2(z_1, t) \right| &\leq \mathcal{B}_2(t, x)|\dot{\phi}_2(s)| \\ &= \mathcal{B}_2(t, x)|0.5\mu_1^2sign(s) \\ &\quad + 1.5\mu_1\mu_2|s|^{1/2}sign(s) + \mu_2^2s| \end{aligned} \tag{32}$$

where $\mathcal{B}_{i=1,2}(t, x) \geq 0$ are known functions.

By using the control law (23), the control sliding mode surface (22) can be re-described as a new system with state (s, φ)

$$\dot{z}_1 = (\tilde{A}_{11} + \tilde{A}_{12}G)z_1 + \tilde{A}_{12}s \tag{33}$$

$$\dot{s} = -\sigma_1\phi_1(s) + \varphi + g_1(z_1, s, t) \tag{34}$$

$$\dot{\varphi} = -\sigma_2\dot{\phi}_2(s) + \dot{g}_2(z_1, t) \tag{35}$$

Note that there exist some positive functions that satisfy $|\Xi_1(x, t)| \leq \mathcal{B}_1(x, t)$ and $|\Xi_2(x, t)| \leq \mathcal{B}_2(x, t)$. In this sense, (31) and (32) can be rewritten as

$$g_1(z_1, s, t) = \Xi_1(x, t)\phi_1(s) \tag{36}$$

$$\dot{g}_2(z_1, t) = \Xi_2(x, t)\dot{\phi}_2(s) \tag{37}$$

Then, a new state vector is introduced

$$\zeta = [\zeta_1 \quad \zeta_2]^T = [\mu_1 |s|^{1/2} \text{sign}(s) + \mu_2 s \quad \varphi]^T \quad (38)$$

Taking $\dot{\phi}_2(s) = \dot{\phi}_1(s)\phi_1(s)$ into account, one obtains

$$\begin{aligned} \dot{\zeta} &= \begin{bmatrix} \dot{\phi}_1(s) \{-\sigma_1 \phi_1(s) + \varphi + g_1(x, t)\} \\ \dot{g}_2(x, t) - \sigma_2 \dot{\phi}_1(s)\phi_1(s) \end{bmatrix} \\ &= \dot{\phi}_1(s) \begin{bmatrix} -(\sigma_1 - \Xi_1(x, t)) & 1 \\ -(\sigma_2 - \Xi_2(x, t)) & 0 \end{bmatrix} \begin{bmatrix} \phi_1(s) \\ \varphi \end{bmatrix} \end{aligned} \quad (39)$$

Defining $\Lambda = \begin{bmatrix} -(\sigma_1 - \Xi_1(x, t)) & 1 \\ -(\sigma_2 - \Xi_2(x, t)) & 0 \end{bmatrix}$, we rewrite (39) as

$$\begin{aligned} \dot{\zeta} &= \begin{bmatrix} \dot{\zeta}_1 \\ \dot{\zeta}_2 \end{bmatrix} \\ &= \dot{\phi}_1(s) \begin{bmatrix} -(\sigma_1 - \Xi_1(x, t)) & 1 \\ -(\sigma_2 - \Xi_2(x, t)) & 0 \end{bmatrix} \zeta \\ &= \dot{\phi}_1(s)\Lambda\zeta \end{aligned} \quad (40)$$

For (38) and (40), it is observed that: (a) if $\zeta_1, \zeta_2 \rightarrow 0$ in finite time then $s, \dot{s} \rightarrow 0$ in finite time; (b) $|\zeta_1| = \mu_1 |s|^{1/2} + \mu_2 |s|$ and $\text{sign}(\zeta_1) = \text{sign}(s)$.

In the second step, we will focus on achieving sufficient conditions for the related variable gains to guarantee Lyapunov stability.

For the reconstructed system (40), choose a candidate Lyapunov function as follows

$$V(s, \varphi) = \zeta^T P \zeta \quad (41)$$

where P denotes a particular symmetric and positive definite matrix, that is to say

$$P = \begin{bmatrix} p_1 & p_3 \\ p_3 & p_2 \end{bmatrix} = P^T > 0 \quad (42)$$

Then, the derivative of the candidate Lyapunov function $V(s, \varphi)$ is determined by

$$\begin{aligned} \dot{V}(s, z) &= \dot{\zeta}^T P \zeta + \zeta^T P \dot{\zeta} \\ &= \dot{\phi}_1(s) \zeta^T \Lambda^T P \zeta + \dot{\phi}_1(s) \zeta^T P \Lambda \zeta \\ &= \dot{\phi}_1(s) \zeta^T (\Lambda^T P + P \Lambda) \zeta \end{aligned} \quad (43)$$

Leaving out the arguments of the functions, one can obtain (44) by substituting P and Λ into $\Lambda^T P + P \Lambda$

$$\begin{aligned} \Lambda^T P + P \Lambda &= \begin{bmatrix} -(\sigma_1 - \Xi_1) & -(\sigma_2 - \Xi_2) \\ 1 & 0 \end{bmatrix} \begin{bmatrix} p_1 & p_3 \\ p_3 & p_2 \end{bmatrix} \\ &+ \begin{bmatrix} p_1 & p_3 \\ p_3 & p_2 \end{bmatrix} \begin{bmatrix} -(\sigma_1 - \Xi_1) & 1 \\ -(\sigma_2 - \Xi_2) & 0 \end{bmatrix} \\ &= \begin{bmatrix} -2p_1(\sigma_1 - \Xi_1) - 2p_3(\sigma_2 - \Xi_2) & * \\ p_1 - p_3(\sigma_1 - \Xi_1) - p_2(\sigma_2 - \Xi_2) & 2p_3 \end{bmatrix} \end{aligned} \quad (44)$$

where $*$ denotes the symmetric element.

It follows from (43) and (44) that

$$\dot{V}(s, z) = -\dot{\phi}_1(s) \zeta^T Q(t, x) \zeta \quad (45)$$

where $Q = -\Lambda^T P - P \Lambda$ denotes a symmetric matrix.

Choosing the elements of positive definite P as $p_1 = \beta + \theta^2, p_2 = 1, p_3 = -\theta$ ($\beta, \theta > 0$) yields

$$\begin{aligned} Q &= \begin{bmatrix} 2(\sigma_1 - \Xi_1)(\beta + \theta^2) - 2\theta(\sigma_2 - \Xi_2) & * \\ (\sigma_1 - \Xi_1)(-\theta) + (\sigma_2 - \Xi_2) - \beta - \theta^2 & 2\theta \end{bmatrix} \\ &= \begin{bmatrix} 2\sigma_1\beta - 2\Xi_1\beta + 2\sigma_1\theta^2 - 2\Xi_1\theta^2 - 2\theta\sigma_2 + 2\theta\Xi_2 & * \\ -\theta\sigma_1 + \theta\Xi_1 + \sigma_2 - \Xi_2 - \beta - \theta^2 & 2\theta \end{bmatrix} \end{aligned} \quad (46)$$

If we select the variable gain σ_2 as

$$\sigma_2 = \beta + \theta^2 + \theta\sigma_1 \quad (47)$$

one can calculate the following matrix inequality

$$\begin{aligned} Q &= \begin{bmatrix} \theta & 0 \\ 0 & \theta \end{bmatrix} \\ &= \begin{bmatrix} 2\sigma_1\beta - 2\Xi_1\beta + 2\sigma_1\theta^2 - 2\Xi_1\theta^2 - 2\theta\sigma_2 + 2\theta\Xi_2 - \theta & * \\ -\theta k_1 + \theta\Xi_1 + \sigma_2 - \Xi_2 - \beta - \theta^2 & \theta \end{bmatrix} \\ &= \begin{bmatrix} 2\sigma_1\beta - 2\Xi_1\beta - 2\Xi_1\theta^2 - 2\theta\beta - 2\theta^3 + 2\theta\Xi_2 - \theta & * \\ \theta\Xi_1 - \Xi_2 & \theta \end{bmatrix} \\ &= \begin{bmatrix} 2\sigma_1\beta - (2\theta + 2\Xi_1)(\beta + \theta^2) + 2\theta\Xi_2 - \theta & * \\ \theta\Xi_1 - \Xi_2 & \theta \end{bmatrix} \end{aligned} \quad (48)$$

To achieve the inequality $Q - \text{diag}(\theta, \theta) \geq 0$, we consider the following Algebraic Riccati Inequality [46]

$$\begin{aligned} \Theta &= 2\sigma_1\beta - (2\theta + 2\Xi_1)(\beta + \theta^2) + 2\theta\Xi_2 \\ &\quad - \theta - (\theta\Xi_1 - \Xi_2) \frac{1}{\theta} (\theta\Xi_1 - \Xi_2) \geq 0 \end{aligned} \quad (49)$$

Based on (31) and (32), a straightforward calculation of (49) leads to

$$\begin{aligned} \sigma_1 &\geq \delta + \frac{1}{\beta} \{(\theta + \mathcal{B}_1)(\beta + \theta^2) + \theta\mathcal{B}_2 \\ &\quad + \frac{1}{2}\theta + \frac{1}{2\theta}(\theta\mathcal{B}_1 + \mathcal{B}_2)^2\} \end{aligned} \quad (50)$$

where $\delta > 0$ denotes an arbitrary positive constant.

Denoting $\lambda\{Q\}$ as the eigenvalue of matrix Q , it can be concluded that (48) is positive definite with the combination (45), (47) and (50), implying that

$$\begin{aligned} \dot{V}(s, z) &= -\dot{\phi}_1(s) \zeta^T Q(t, x) \zeta \\ &\leq -\lambda_{\min}\{Q\} \dot{\phi}_1(s) \zeta^T \zeta \\ &\leq -\theta \dot{\phi}_1(s) \|\zeta\|_2^2 \end{aligned} \quad (51)$$

Since

$$\begin{aligned} \dot{\phi}_1(s) &= (u_1 |s|^{-1/2} + u_2) \geq 0 \\ \|\zeta\|_2^2 &= \phi_1^2 + \varphi^2 = \mu_1^2 |s| + 2\mu_1\mu_2 |s|^{3/2} + \mu_2^2 s^2 + \varphi^2 \end{aligned} \quad (52)$$

it is concluded from (51) that the stability of the resultant system is guaranteed. This completes the proof.

Theorem 2: Suppose that $\sigma_1 > 0$ and $\sigma_2 > 0$ satisfying (47) and (50), and generally $u_2 \geq 0$. The proposed RSSMC method and Theorem 1 ensure that the states of the FAMR system will be driven to the origin within a finite time, and the upper bound of the convergence time can be estimated.

Proof: Let us consider the following quadratic inequality

$$\lambda_{\min}\{P\} \|\zeta\|_2^2 \leq \zeta^T P \zeta \leq \lambda_{\max}\{P\} \|\zeta\|_2^2 \quad (54)$$

The combination of (41) and (54) leads to

$$\mu_1 |s|^{1/2} \leq \|\zeta\|_2 \leq \frac{V^{1/2}(s, \varphi)}{\lambda_{\min}^{1/2}\{P\}}, \frac{V^{1/2}(s, \varphi)}{\lambda_{\max}^{1/2}\{P\}} \leq \|\zeta\|_2 \quad (55)$$

Further, it is possible to write (51) as

$$\begin{aligned} \dot{V}(s, \varphi) &\leq -\theta \left(\mu_1^2 \frac{1}{2\mu_1 |s|^{1/2}} + \mu_2 \right) \|\zeta\|_2^2 \\ &\leq -\frac{\theta \mu_1^2 \lambda_{\min}^{1/2}\{P\}}{2\lambda_{\max}\{P\}} V^{1/2}(s, \varphi) - \frac{\theta \mu_2}{\lambda_{\max}\{P\}} V(s, \varphi) \end{aligned} \quad (56)$$

From (56), we can conclude that $V(s, \varphi)$ is ensured to be continuously decreased, converging to the equilibrium point $(s, \varphi) = 0$ in finite time under arbitrary initial condition. For the convergence time analysis, define

$$\gamma_1(\mu_1) = \frac{\theta \mu_1^2 \lambda_{\min}^{1/2}\{P\}}{2\lambda_{\max}\{P\}}, \quad \gamma_2(\mu_2) = \frac{\theta \mu_2}{\lambda_{\max}\{P\}} \quad (57)$$

The derivation of the following differential formulation

$$\dot{v}(t) = -\gamma_1(\mu_1)v(t)^{1/2} - \gamma_2(\mu_2)v(t), \quad v(0) = v_0 > 0 \quad (58)$$

is determined by

$$v(t) = \left(v_0^{1/2} - \frac{\gamma_1(\mu_1)}{2} t \right)^2, \quad \text{if } \gamma_1 = 1, \gamma_2 = 0 \quad (59)$$

or, when if $\gamma_1 \geq 1, \gamma_2 > 0$

$$\begin{aligned} v(t) &= \exp(-\gamma_2(\mu_2)t) \\ &\times \left[v_0^{1/2} + \frac{\gamma_1(\mu_1)}{\gamma_2(\mu_2)} \left(1 - \exp\left(\frac{\gamma_2(\mu_2)}{2} t\right) \right) \right]^2 \end{aligned} \quad (60)$$

It follows from (56) that $V(t) \leq v(t)$ when $V(s_0, \varphi_0) \leq v_0$. Therefore, s will be driven to the origin within finite time. To be more specific, the reaching time can be estimated by

$$T = \begin{cases} \frac{2}{\gamma_1(\mu_1)} V^{1/2}(s_0, \varphi_0) & \text{if } u_2 = 0 \\ \frac{2}{\gamma_2(\mu_2)} \ln \left(\frac{\gamma_2(\mu_2)}{\gamma_1(\mu_1)} V^{1/2}(s_0, \varphi_0) + 1 \right) & \text{if } u_2 > 0 \end{cases} \quad (61)$$

Therefore, under the designed variable gains determined by (47) and (50), s and \dot{s} converge to the origin in finite time which can be estimated by (61). This confirms the finite time convergence of the resultant FAMR system. The proof is completed.

Finally, Figure 3 shows the proposed control framework, and the implementation procedure can be summarized as:

- Step 1: Construct the reference vehicle mode based on (16) and (17);
- Step 2: Obtain the corresponding tracking errors using the related yaw rate and sideslip angle;
- Step 3: Determine the desired sliding surface with (22);

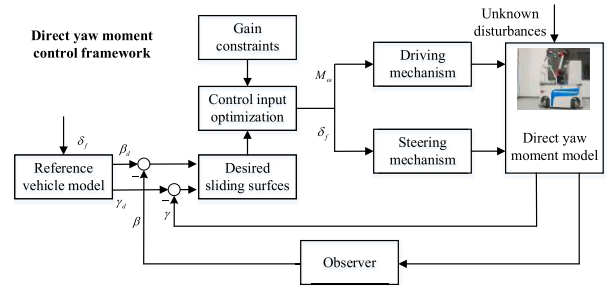


FIGURE 3. The proposed control framework.

Step 4: Together with the control gain constraints, optimize the control input M_ω and δ_f ;

Step 5: Control the FAMR system using the designed driving and steering mechanisms;

Remark 2: As can be seen from (1) and (2), the FAMR system considered in this paper is a nonlinear multi-inputs multi-outputs system. With the help of small-angle approximation, we modify the original system as linear systems. It is worth mentioning that this method is applicable for the control of general nonlinear system with multiple inputs/outputs. For practical implementations, by using the linearized method (such as the studies in [47]), the multi-inputs multi-outputs nonlinear system can be transformed into a system in Brunowsky canonical form, and then the original nonlinear system can be expressed as a linear one. Given this context, the proposed method is still applicable for such a transferred nonlinear system, validating the practicability of the proposed method.

Remark 3: At this point, compared to the existing designs, we will demonstrate the distinguishing features of the presented RSSMC method. Firstly, the newly proposed method is applicable for trajectory tracking control of very universal systems subject to external disturbances and uncertainties states, including the linear systems and nonlinear ones. In this regard, the “ideal modelling” assumption is not necessary during the derivation of the proposed RSSMC method. Although the upper limit of the system uncertainties is required, we can easily obtain the necessary information since the main disturbances of the FAMR are caused by the time-varying inertia and payload. Moreover, the undesired chattering is accommodated by using a continuous SMC controller instead of universal adopted discontinuous ones based on a multivariable super-twisting mechanism. The multiple disturbances can be rejected with continuous control inputs. Finally, the overestimated issue of the control parameters can be well addressed since the related gains are suitably tuned based on the stability and convergence aspects.

Remark 4: This paper mainly concerns the direct yaw moment regulation issue of FAMR systems subject to unknown disturbances and system uncertainties. For practical autonomous mobile robots, unmeasurable velocities, input saturation, etc., are commonly occurred during the control process. These may reduce the control qualities of the closed-loop system. Note that saturation functions and quasi

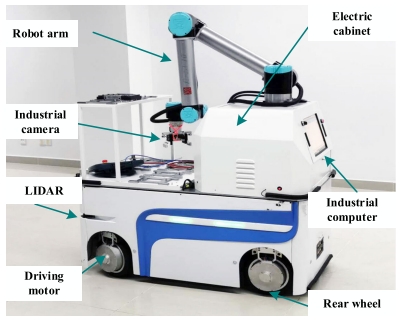


FIGURE 4. The developed FAMR.

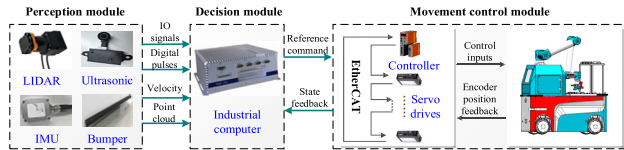


FIGURE 5. Hardware architecture.

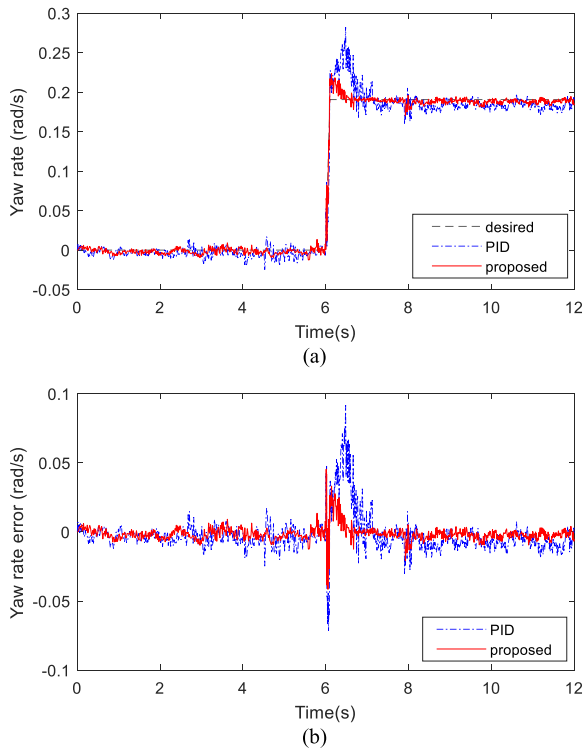


FIGURE 6. Yaw rate tracking results of case 1. (a) yaw rate; (b) the corresponding tracking errors.

velocities can be utilized to provide effective solutions for the above-mentioned challenges. For example, the partial saturation function is considered to handle the tire force saturation of the mobile robots, and the integral sliding mode mechanism is used to mitigate the input saturation issue [48]. These challenges will be interesting topics for further explorations.

IV. EXPERIMENTAL RESULTS AND ANALYSIS

A. EXPERIMENTAL SETUP

For simulation experimental validation, the proposed RSSMC method is realized using a developed platform

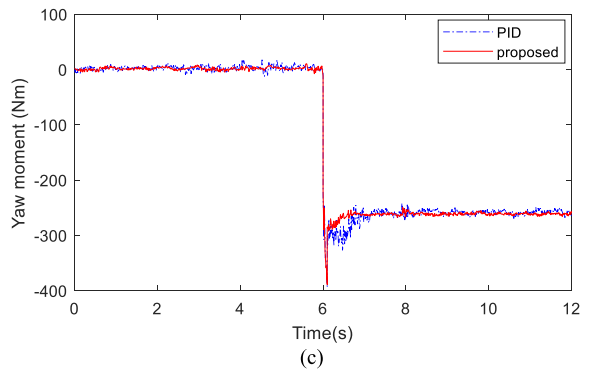
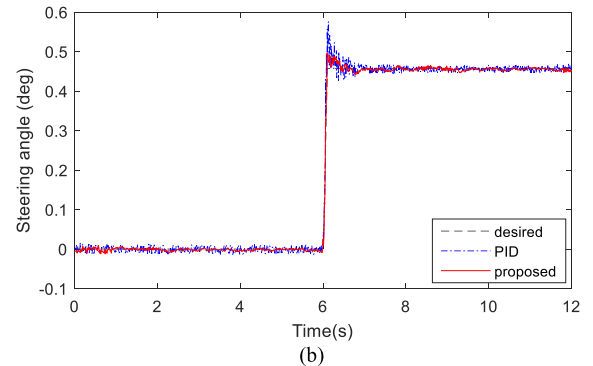
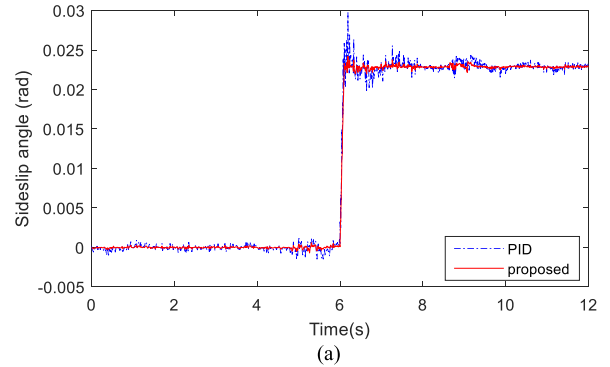


FIGURE 7. The related signals of case 1. (a) sideslip angle; (b) steering angle δ_f ; (c) yaw moment.

shown in Figure 4. For onboard equipment, the developed FAMR is equipped with an electric cabinet, industrial computer, laser (rangefinders, HOKUYO UTM-30LX), industrial camera, and a robot arm. This FAMR has several prominent features, such as automatic charging, trackless autonomous navigation, anti-crash measurements and vision-based operating the workpiece. It has been applied to industrial manufacturing applications to perform locomotion and manipulation synchronously. Owing to the independently-driving independently-steering property, each wheel has two degree-of-freedom to achieve active arbitrary movements and rotation. To summarize, the hardware architecture contains the modules of: (1) perception, used to obtain the sensory data for perceiving the real-world surrounding and guaranteeing the safety of the robot in unmapped or dynamic environments; (2) decision making, used for global localization, pose estimation and formulating strategies for next

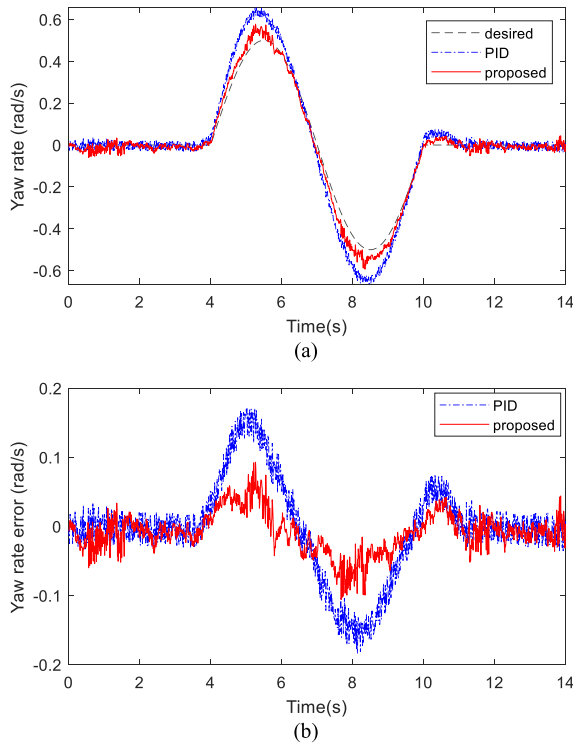


FIGURE 8. Yaw rate tracking results of case 2. (a) yaw rate; (b) corresponding tracking errors.

actions; (3) movement control, implementing the actuation functions to achieve yaw moment control.

For simulation experimental implementation, the key specifications of the developed FAMR platform are: $l_f = l_r = 0.445m$, $d = 0.53m$. The normal road adhesion coefficient is determined as $\mu = 0.9$. The reduction radii of the driving motor and steering motor are 7.6 and 60, respectively. Further, we set $\mu_1 = 0.5$, $\mu_2 = 1$, $\theta = 0.3$, $\beta = 1$, $\delta = 0.01$. For comparison reason, we apply the traditional proportional-integral-derivative (PID) controller tuned by trial and error. The related parameters are determined by $\{k_p = 1.0, k_i = k_d = 0.9\}$. The sampling time is specified as 0.001s.

B. SIMULATION EXPERIMENTAL RESULTS

For simulation validation, we will consider the typical ramp steering and double-changing maneuvers under different modes. The above maneuvers will be generally-applied to access the lateral control performance in a nonidealized working environment. It is worth mentioning that the widely used traditional Ackerman and double-Ackerman modes are considered to verify the practicability of the newly developed RSSMC scheme. The anti-disturbance trajectory tracking in a complex operating environment is considered with the ground disturbed by oil/water. In practice, the control performances will be affected by disturbances, including system parameter uncertainty, external noise and unmodeled dynamics. Furthermore, the movement of the mounted robot arm will impose additional external disturbances for the chassis control module of the FAMR system. Then, comparison

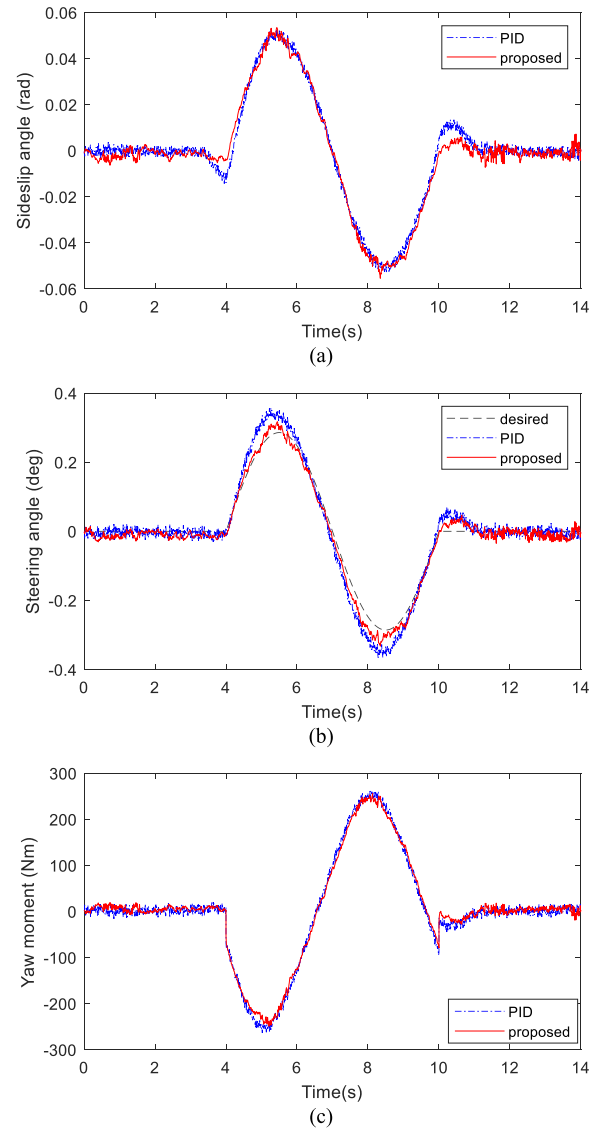


FIGURE 9. The related signals of case 2. (a) sideslip angle; (b) steering angle; (c) yaw moment.

simulation experiments are conducted with respect to different desired trajectories and operational modes. In this regard, we provide the following cases for demonstration.

Case 1) Ramp steering control under Ackerman mode

In this case, we will pay attention to the ramp steering control with the commonly-used Ackerman mode. The reference yaw rate increases from zero to near 0.2 rad/s within 0.1 s, and keeps the yaw rate for the subsequent periods. The results of the dynamic response and related tracking errors during the ramp steering maneuver are shown in Figure 6 (a) and (b), separately. As depicted in these corresponding evaluations, our presented RSSMC scheme is capable of achieving improved ramp responses as compared to the traditional method. As it can be observed, there are no steady-state errors in the resulting systems under the comparison control scheme. Note that our proposed method possesses better performance in terms of overshoot and settling time. To be more

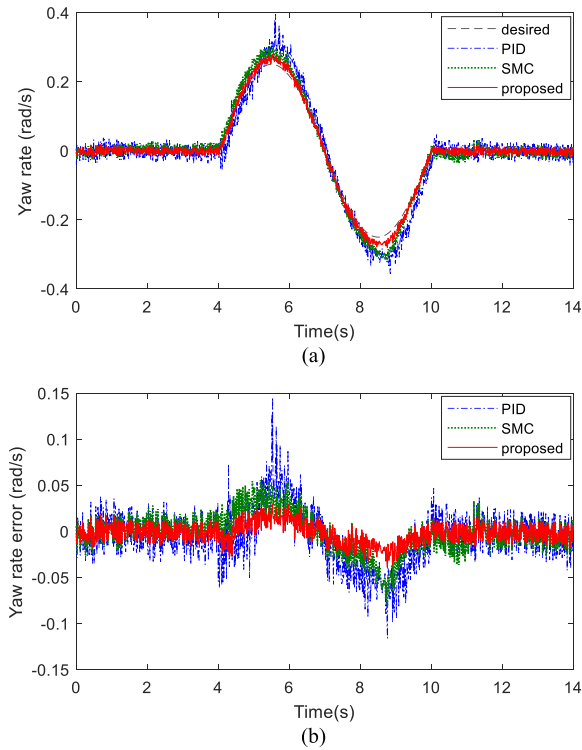


FIGURE 10. Yaw rate tracking results of case 3. (a) yaw rate; (b) corresponding tracking errors.

specific, the system under the control of our RSSMC method has enhanced rise time (0.0803 s) and overshoot mitigation (17.42%) capacity. In comparison, the rise time and overshoot of the traditional method are 0.0934 s and 48.18%, respectively, which may affect the lateral motion control stability and dynamic tracking accuracy and efficiency.

Figure 7 shows the corresponding signals related to this case, including the sideslip angle, steering angle and yaw moment inputs during the ramp steering maneuver. After careful observation, we conclude that there exist more distinct oscillations in the transient process of the resultant system under the traditional method, whereas our proposed RSSMC scheme is able to mitigate the impact of disturbances and provides the smaller errors around the origin, therefore yielding a better tracking performance.

Case 2) Tracking control under Ackerman mode

To test the robustness of the resulted system under the widely applied Ackerman mode, the sinusoidal steering profile is considered here. The corresponding responses and signals are shown in Figures 7 and 8.

Figure 7 (a) and (b) describe the yaw rate responses and the corresponding errors, respectively. As shown in Figure 7, both the presented RSSMC and the traditional method can lead to stable lateral motion responses. Further, as can be seen from Figure 8 (b), the tracking error of the system under the traditional PID control scheme has larger amplitudes. This is caused by the vibrations of the tracking profiles and lumped disturbances. In comparison, the proposed RSSMC scheme is able to follow the desired yaw rate with better accuracy and smoother responses.

TABLE 1. The performance criteria of the yaw rate error under the comparison controllers.

Case number	Method	Criteria		
		Max	IAE	ISE
Case 1	PID	0.0918	0.1022	0.0022
	proposed	0.0454	0.0432	0.0004
Case 2	PID	0.1837	0.6712	0.0672
	proposed	0.1058	0.3154	0.0131
Case 3	PID	0.1453	0.3212	0.0127
	SMC	0.0806	0.2252	0.0063
	proposed	0.0401	0.1271	0.0018

Figure 9 illustrates the related signals in terms of the sideslip angle, steering angle, and yaw moment using the traditional PID controller and our presented RSSMC method. Unlike the newly developed method, the traditional PID controller will result in non-negligible overshoots. Due to the external disturbance and unknown uncertainties, some vibration changes with tremendous amplitude are also observed in the traditional control system. Intuitively, the presented RSSMC method offers more robustness against the unknown disturbances such that the system performs closely as the reference profiles.

In conclusion, the simulation experimental results derived from this case show the proposed RSSMC controller under Ackerman mode is capable of efficaciously alleviating the negative effects of the lumped disturbances and uncertainties, and obtain direct yaw moment control with high precision when performing lateral motion control.

Case 3) Tracking control under double-Ackerman mode

For simulation verification of the proposed RSSMC method under another widely used configuration mode, i.e., double-Ackerman mode, we carry out this case with a single-lane change maneuver. It should also be noted that the traditional SMC method that adopts reaching law with a constant term for comparison [12]. As can be observed from Figure 10 and Figure 11, the test results are in line with the theoretical analysis. Our presented RSSMC, traditional PID and SMC methods can obtain stable responses for tracking the desired yaw rate and constraining the sideslip angle. For a fair comparative case, the RSSMC method outperforms the traditional control schemes, which can enable the resultant FAMR system with smoother dynamics and enhanced stability. As shown in Figure 10 (b), the yaw rate tracking errors are ensured to be within a small range around zero, implying a satisfactory motion response. There exist some vibrations of the tracking errors caused by the unknown disturbances, such as unmodelled dynamics, uncertainties and external disturbances. The results show that the disturbances will diminish the performance quality of the controller system and the proposed method obtains smaller tracking error than other controllers.

On the other hand, according to the comparative evaluations demonstrated in Figure 11, we know that the proposed method can make the FAMR effectively to achieve smoother

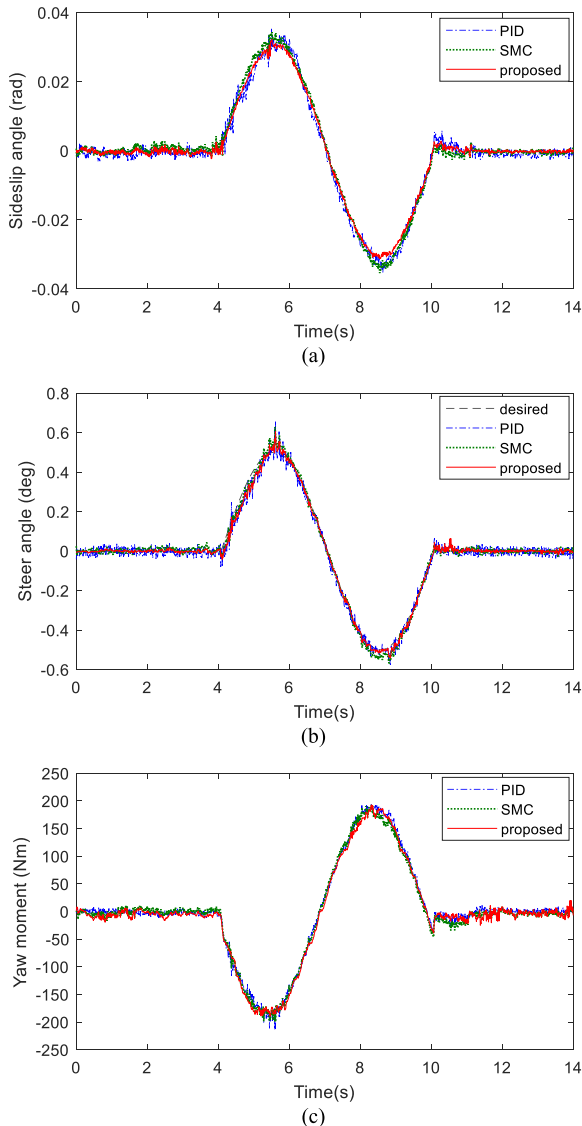


FIGURE 11. The related signals of case 2. (a) sideslip angle; (b) steering angle δ_f ; (c) yaw moment.

responses. Therefore, by applying the proposed method using the double-Ackerman mode, the lateral stability motion control is realized to follow the related reference profiles with guaranteed precision.

Further, using the obtained absolute value of the tracking errors in the mentioned three cases, we have calculated the performance criteria in terms of the maximum value, the integral absolute error (IAE) and the integral squared error (ISE). It should be mentioned that, the IAE has long been employed as a response indicator concerning sustained oscillation. A resultant system with better ISE performance can achieve quick responses since minimizing the ISE is helpful for alleviating large tracking errors faster. Further, as depicted in TABLE 1, as compared to the traditional PID method, by applying the proposed RSSMC method, the considered criteria concerning IAE and ISE are improved by (57.73%, 81.81%), (53.01%, 80.51%), and (60.43%, 85.83%)

in cases 1, 2 and 3, separately. On other hand, as compared to the conventional SMC method, the related criteria (Max, IAE and ISE) of the resultant system under the proposed RSSMC method can be reduced by 50.25%, 43.56%, and 71.43%, respectively. From these results, once can conclude that our proposed method is potential for enhancing the direct yaw moment control of the FAMR with improved tracking and anti-disturbance performance in various operating environments.

V. CONCLUSION AND FUTURE WORKS

This paper proposes an improved RSSMC scheme to reach the anti-disturbance direct yaw moment control of a home-developed FAMR. Under lumped disturbances and uncertainties, the proposed scheme is capable of scheduling the yaw rate and sideslip angle simultaneously. To eliminate the matched perturbations and time-varying lumped disturbances, a modified sliding mode mechanism is designed with attractive characteristics: continuous control input, finite-time convergence and enhanced robustness. This guarantees that the system outputs can arrive at the desired sliding region asymptotically, which achieves better control precision in both the sliding motion phase and reaching phase. New sufficient conditions of the concerned multivariable gains are explored with the help of algebra Lyapunov functions so that the resultant FAMR system can be stabilized globally. Comparative simulation experiments are performed and the related results validate that the direct yaw moment control performance of the FAMR system can be significantly improved. As can be seen from the simulation experimental results, the proposed method is able to enhance the dynamic tracking performance and robustness against the unknown disturbance simultaneously. It is then concluded that the presented RSSMC method could certainly satisfy the stringent requirements of practical FAMR implementations.

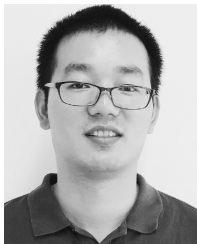
It should be pointed out that the developed FAMR can operate in multiple kinematic allocations as a profit of its independently steering and driving feature. The switching control between multi-modes will be investigated in the future to makes full use of the configuration advantages of FAMR such that the developed FAMR can track the reference trajectories with more maneuverability and mobility in the confined spaces or dynamic environments. As another extension of the proposed method, the disturbance rejection issue of a nonlinear system (including the multi-inputs multi-outputs system) can be well handled with the newly-designed sliding mode mechanism.

REFERENCES

- [1] M. A. Kamel, X. Yu, and Y. Zhang, "Fault-tolerant cooperative control design of multiple wheeled mobile robots," *IEEE Trans. Control Syst. Technol.*, vol. 26, no. 2, pp. 756–764, Mar. 2018.
- [2] B. Ning, Q.-L. Han, Z. Zuo, J. Jin, and J. Zheng, "Collective behaviors of mobile robots beyond the nearest neighbor rules with switching topology," *IEEE Trans. Cybern.*, vol. 48, no. 5, pp. 1577–1590, May 2018.
- [3] X. Jin, "Fault-tolerant iterative learning control for mobile robots non-repetitive trajectory tracking with output constraints," *Automatica*, vol. 94, pp. 63–71, 2018.

- [4] D. Rotondo, V. Puig, F. Nejari, and J. Romera, "A fault-hiding approach for the switching quasi-LPV fault-tolerant control of a four-wheeled omnidirectional mobile robot," *IEEE Trans. Ind. Electron.*, vol. 62, no. 6, pp. 3932–3944, Jun. 2015.
- [5] A. Jaskot, B. Posiadała, and S. Āšpiwák, "Dynamics modelling of the four-wheeled mobile platform," *Mech. Res. Commun.*, vol. 83, pp. 58–64, Jul. 2017.
- [6] X. Zhang, Y. Xie, L. Jiang, G. Li, J. Meng, and Y. Huang, "Fault-tolerant dynamic control of a four-wheel redundantly-actuated mobile robot," *IEEE Access*, vol. 7, pp. 157909–157921, 2019.
- [7] B. Tao, X. W. Zhao, and H. Ding, "Mobile-robotic machining for large complex components: A review study," *Sci. China Technol. Sci.*, vol. 62, pp. 1–13, Oct. 2019.
- [8] Y. Wu, P. Balatti, M. Lorenzini, F. Zhao, W. Kim, and A. Ajoudani, "A teleoperation interface for loco-manipulation control of mobile collaborative robotic assistant," *IEEE Robot. Autom. Lett.*, vol. 4, no. 4, pp. 3593–3600, Oct. 2019.
- [9] J. S. Keek, S. L. Loh, and S. H. Chong, "Comprehensive development and control of a path-trackable mecatronics-wheeled robot," *IEEE Access*, vol. 7, pp. 18368–18381, 2019.
- [10] Z. Yuan, Y. Tian, Y. Yin, S. Wang, J. Liu, and L. Wu, "Trajectory tracking control of a four mecatronics-wheeled mobile platform: An extended state observer-based sliding mode approach," *IET Control Theory Appl.*, vol. 14, no. 3, pp. 415–426, Feb. 2020.
- [11] Y. Yu, L. Zhao, and C. Zhou, "Influence of rotor-bearing coupling vibration on dynamic behavior of electric vehicle driven by in-wheel motor," *IEEE Access*, vol. 7, pp. 63540–63549, 2019.
- [12] Y. Xie, X. Zhang, W. Meng, S. Zheng, L. Jiang, J. Meng, and S. Wang, "Coupled fractional-order sliding mode control and obstacle avoidance of a four-wheeled steerable mobile robot," *ISA Trans.*, Aug. 2020, doi: 10.1016/j.isatra.2020.08.025.
- [13] D. Zhang, G. Liu, H. Zhou, and W. Zhao, "Adaptive sliding mode fault-tolerant coordination control for four-wheel independently driven electric vehicles," *IEEE Trans. Ind. Electron.*, vol. 65, no. 11, pp. 9090–9100, Nov. 2018.
- [14] L. Zhang, Y. Wang, and Z. Wang, "Robust lateral motion control for In-Wheel-Motor-Drive electric vehicles with network induced delays," *IEEE Trans. Veh. Technol.*, vol. 68, no. 11, pp. 10585–10593, Nov. 2019.
- [15] Z. Li, L. Zheng, W. Gao, and Z. Zhan, "Electromechanical coupling mechanism and control strategy for In-Wheel-Motor-Driven electric vehicles," *IEEE Trans. Ind. Electron.*, vol. 66, no. 6, pp. 4524–4533, Jun. 2019.
- [16] X. Liang, H. Wang, Y.-H. Liu, W. Chen, and Z. Jing, "Image-based position control of mobile robots with a completely unknown fixed camera," *IEEE Trans. Autom. Control*, vol. 63, no. 9, pp. 3016–3023, Sep. 2018.
- [17] Y. Wang, D. Wang, S. Yang, and M. Shan, "A practical leader-follower tracking control scheme for multiple nonholonomic mobile robots in unknown obstacle environments," *IEEE Trans. Control Syst. Technol.*, vol. 27, no. 4, pp. 1685–1693, Jul. 2019.
- [18] J. Liao, Z. Chen, and B. Yao, "Model-based coordinated control of four-wheel independently driven skid steer mobile robot with wheel-ground interaction and wheel dynamics," *IEEE Trans. Ind. Informat.*, vol. 15, no. 3, pp. 1742–1752, Mar. 2019.
- [19] Y. Xie, X. Zhang, W. Meng, S. Xie, L. Jiang, J. Meng, and S. Wang, "Coupled sliding mode control of an omnidirectional mobile robot with variable modes," in *Proc. IEEE/ASME Int. Conf. Adv. Intell. Mechatronics (AIM)*, Boston, MA, USA, Jul. 2020, pp. 1792–1797.
- [20] R. Wang, C. Hu, F. Yan, and M. Chadli, "Composite nonlinear feedback control for path following of four-wheel independently actuated autonomous ground vehicles," *IEEE Trans. Intell. Transp. Syst.*, vol. 17, no. 7, pp. 2063–2074, Jul. 2016.
- [21] J. Ni, J. Hu, and C. Xiang, "Envelope control for four-wheel independently actuated autonomous ground vehicle through AFS/DYC integrated control," *IEEE Trans. Veh. Technol.*, vol. 66, no. 11, pp. 9712–9726, Nov. 2017.
- [22] C. Lin, S. Liang, J. Chen, and X. Gao, "A multi-objective optimal torque distribution strategy for four In-Wheel-Motor drive electric vehicles," *IEEE Access*, vol. 7, pp. 64627–64640, 2019.
- [23] J.-S. Hu, Y. Wang, H. Fujimoto, and Y. Hori, "Robust yaw stability control for in-wheel motor electric vehicles," *IEEE/ASME Trans. Mechatronics*, vol. 22, no. 3, pp. 1360–1370, Jun. 2017.
- [24] Y. Song, H. Shu, X. Chen, and S. Luo, "Direct-yaw-moment control of four-wheel-drive electric vehicle based on lateral tyre-road forces and sideslip angle observer," *IET Intell. Transp. Syst.*, vol. 13, no. 2, pp. 303–312, Feb. 2019.
- [25] P. Zhang, J. Hu, H. Liu, and C. Zhang, "Sliding mode control for networked systems with randomly varying nonlinearities and stochastic communication delays under uncertain occurrence probabilities," *Neurocomputing*, vol. 320, pp. 1–11, Dec. 2018.
- [26] Y. Han, Y. Kao, and C. Gao, "Robust sliding mode control for uncertain discrete singular systems with time-varying delays and external disturbances," *Automatica*, vol. 75, pp. 210–216, Jan. 2017.
- [27] J. Zhang, H. Wang, J. Zheng, Z. Cao, Z. Man, M. Yu, and L. Chen, "Adaptive sliding mode-based lateral stability control of steer-by-wire vehicles with experimental validations," *IEEE Trans. Veh. Technol.*, early access, Jun. 18, 2020, doi: 10.1109/TVT.2020.3003326.
- [28] J. Hu, Y. Cui, C. Lv, D. Chen, and H. Zhang, "Robust adaptive sliding mode control for discrete singular systems with randomly occurring mixed time-delays under uncertain occurrence probabilities," *Int. J. Syst. Sci.*, vol. 51, no. 6, pp. 987–1006, Apr. 2020.
- [29] J. Hu, P. Zhang, Y. Kao, H. Liu, and D. Chen, "Sliding mode control for Markovian jump repeated scalar nonlinear systems with packet dropouts: The uncertain occurrence probabilities case," *Appl. Math. Comput.*, vol. 362, Dec. 2019, Art. no. 124574.
- [30] S. Ding and J. Sun, "Direct yaw-moment control for 4WID electric vehicle via finite-time control technique," *Nonlinear Dyn.*, vol. 88, no. 1, pp. 239–254, Apr. 2017.
- [31] T. Goggia, A. Sorniotti, L. De Novellis, A. Ferrara, P. Gruber, J. Theunissen, D. Steenbeke, B. Knauder, and J. Zehetner, "Integral sliding mode for the torque-vectoring control of fully electric vehicles: Theoretical design and experimental assessment," *IEEE Trans. Veh. Technol.*, vol. 64, no. 5, pp. 1701–1715, May 2015.
- [32] J. Ni, J. Hu, and C. Xiang, "Robust control in diagonal move steer mode and experiment on an X-by-Wire UGV," *IEEE/ASME Trans. Mechatronics*, vol. 24, no. 2, pp. 572–584, Apr. 2019.
- [33] J. Ni, J. Hu, and C. Xiang, "An AWID and AWIS X-By-Wire UGV: Design and hierarchical chassis dynamics control," *IEEE Trans. Intell. Transp. Syst.*, vol. 20, no. 2, pp. 654–666, Feb. 2019.
- [34] M. A. Jaradat, M. Bani-Salim, and F. Awad, "A highly-maneuverable demining autonomous robot: An over-actuated design," *J. Intell. Robot. Syst.*, vol. 90, nos. 1–2, pp. 65–80, May 2018.
- [35] K. Nam, H. Fujimoto, and Y. Hori, "Lateral stability control of In-Wheel-Motor-Driven electric vehicles based on sideslip angle estimation using lateral tire force sensors," *IEEE Trans. Veh. Technol.*, vol. 61, no. 5, pp. 1972–1985, Jun. 2012.
- [36] P. Dai and J. Katupitiya, "Force control for path following of a 4WS4WD vehicle by the integration of PSO and SMC," *Vehicle Syst. Dyn.*, vol. 56, no. 11, pp. 1682–1716, Nov. 2018.
- [37] K. Nam, S. Oh, H. Fujimoto, and Y. Hori, "Estimation of sideslip and roll angles of electric vehicles using lateral tire force sensors through RLS and Kalman filter approaches," *IEEE Trans. Ind. Electron.*, vol. 60, no. 3, pp. 988–1000, Mar. 2013.
- [38] P. Singh, P. Agrawal, H. Karki, A. Shukla, N. K. Verma, and L. Behera, "Vision-based guidance and switching-based sliding mode controller for a mobile robot in the cyber physical framework," *IEEE Trans. Ind. Informat.*, vol. 15, no. 4, pp. 1985–1997, Apr. 2019.
- [39] Y. Zhao, F. Zhang, P. Huang, and X. Liu, "Impulsive super-twisting sliding mode control for space debris capturing via tethered space net robot," *IEEE Trans. Ind. Electron.*, vol. 67, no. 8, pp. 6874–6882, Aug. 2020.
- [40] S. M. Mozayan, M. Saad, H. Vahedi, H. Fortin-Blanchette, and M. Soltani, "Sliding mode control of PMSG wind turbine based on enhanced exponential reaching law," *IEEE Trans. Ind. Electron.*, vol. 63, no. 10, pp. 6148–6159, Oct. 2016.
- [41] A. Wang and S. Wei, "Sliding mode control for permanent magnet synchronous motor drive based on an improved exponential reaching law," *IEEE Access*, vol. 7, pp. 146866–146875, 2019.
- [42] Z. Shuai, H. Zhang, J. Wang, J. Li, and M. Ouyang, "Combined AFS and DYC control of Four-Wheel-Independent-Drive electric vehicles over CAN network with time-varying delays," *IEEE Trans. Veh. Technol.*, vol. 63, no. 2, pp. 591–602, Feb. 2014.
- [43] I. Nagesh and C. Edwards, "A multivariable super-twisting sliding mode approach," *Automatica*, vol. 50, no. 3, pp. 984–988, Mar. 2014.
- [44] T. Gonzalez, J. A. Moreno, and L. Fridman, "Variable gain super-twisting sliding mode control," *IEEE Trans. Autom. Control*, vol. 57, no. 8, pp. 2100–2105, Aug. 2012.
- [45] K. Liao and Y. Xu, "A robust load frequency control scheme for power systems based on second-order sliding mode and extended disturbance observer," *IEEE Trans. Ind. Informat.*, vol. 14, no. 7, pp. 3076–3086, Jul. 2018.

- [46] F. J. Vargas and R. A. Gonzalez, "On the existence of a stabilizing solution of modified algebraic Riccati equations in terms of standard algebraic Riccati equations and linear matrix inequalities," *IEEE Control Syst. Lett.*, vol. 4, no. 1, pp. 91–96, Jan. 2020.
- [47] S. Mondal and C. Mahanta, "A fast converging robust controller using adaptive second order sliding mode," *ISA Trans.*, vol. 51, no. 6, pp. 713–721, Nov. 2012.
- [48] C. Hu, R. Wang, and F. Yan, "Integral sliding mode-based composite nonlinear feedback control for path following of four-wheel independently actuated autonomous vehicles," *IEEE Trans. Transport. Electrific.*, vol. 2, no. 2, pp. 221–230, Jun. 2016.



LIQUAN JIANG received the B.S. degree in mechanical engineering from the China University of Geosciences, Wuhan, China, in 2014, the M.S. degree in mechanical and electronic engineering from the Huazhong University of Science and Technology, Wuhan, China, in 2017, where he is currently pursuing the Ph.D. degree with the School of Mechanical Science and Engineering.

His research interests include optimization algorithms, robot control, and path planning.



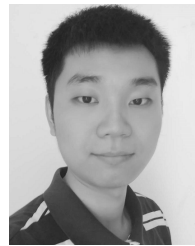
SHUTING WANG received the B.S. and M.S. degrees from the School of Energy and Power Engineering, Wuhan University of Technology, Wuhan, China, in 1991 and 1994, respectively, and the Ph.D. degree from the School of Mechanical Science and Engineering, Huazhong University of Science and Technology (HUST), Wuhan, in 2002.

He is currently a Full Professor and the Vice-President of the School of Mechanical Science and Engineering, HUST, where he is also the Deputy Director of the National CAD Support Software Engineering Research Center. He has published more than 90 articles. His research interests include mobile robot, mechanical design, and numerical control.



YUANLONG XIE (Member, IEEE) received the B.S. degree in electrical engineering and the Ph.D. degree in mechanical engineering from the Huazhong University of Science and Technology (HUST), Wuhan, China, in 2014 and 2018, respectively.

He was an Academic Visitor with the School of Electronic and Electrical Engineering, University of Leeds, Leeds, U.K., from 2017 to 2018. He has been a Postdoctoral Fellow with HUST, since November 2018. He has published more than 40 academic journal and conference papers, and holds more than ten patents. His research interests include robot control, servo control, field-bus technology, and networked control systems.



JIE MENG received the B.S. degree in mechanical engineering from the Wuhan University of Technology, Wuhan, China, in 2016. He is currently pursuing the Ph.D. degree with the School of Mechanical Science and Engineering, Huazhong University of Science and Technology, Wuhan.

He has published four academic journal and conference papers, and holds two patents. His research interests include robot perception and mobile robot navigation.



SHIQI ZHENG received the Ph.D. degree from the School of Mechanical Science and Engineering, Huazhong University of Science and Technology, Wuhan, China, in 2016.

He was an Academic Visitor with the School of Electrical and Electronic Engineering, The University of Adelaide, Adelaide, Australia, from 2018 to 2019. He is currently an Associate Professor with the China University of Geosciences, Wuhan. His current research interests include adaptive and

robust control for complex systems, such as switched systems, multiagent systems, and fractional order systems.

Dr. Zheng has been a Reviewer of the *Journal of the Franklin Institute* and the *International Journal of Robust and Nonlinear Control*.



XIAOLONG ZHANG (Student Member, IEEE) received the master's degree in mechanical engineering from the Huazhong University of Science and Technology (HUST), Wuhan, China, in 2015, where he is currently pursuing the Ph.D. degree with the School of Mechanical Science and Engineering.

His research interests include mobile robot, robot control, and motion planning.



HAO WU received the B.S. degree from the School of Mechanical and Electrical Engineering, Wuhan University of Technology, in 2017, and the M.S. degree in mechanical engineering from the Huazhong University of Science and Technology, Wuhan, China, in 2020, where he is currently pursuing the Ph.D. degree with the School of Mechanical Science and Engineering.

His research interests include robot control and path planning.

...